Can Structural MRI Indices of Cerebral Integrity Track Cognitive Trends in Executive Control Function During Normal Maturation and Adulthood?

Peter Kochunov,[1]* Don A. Robin,[1] Don R. Royall,[2] Thomas Coyle,[3] Jack Lancaster,[1] Valeria Kochunov,[1] Anita E. Schlosser,[1] and Peter T. Fox[1]

[1]*Research Imaging Center, University of Texas Health Science Center at San Antonio, Texas*
[2]*Department of Psychiatry, University of Texas Health Science Center at San Antonio, Texas*
[3]*Department of Psychology, University of Texas at San Antonio, Texas*

Abstract: We explored the relationship between structural neuroimaging-based indices of cerebral integrity and executive control function (ECF) in two groups of healthy subjects: A maturing group (33 subjects; 19–29 years) and a senescing group (38 adults; 30–90 years). ECF was assessed using the Executive Interview (EXIT) battery. Cortical indices of cerebral integrity included GM thickness, intergyral span, and sulcal span, each measured for five cortical regions per hemisphere. Subcortical indices included fractional anisotropy (FA), measured using track-based-spatial-statistics (TBSS), and the volume of T2-hyperintense WM (HWM). In the maturing group, no significant relationships between neuroanatomical changes and ECF were found; however, there were hints that late-term maturation of cerebral WM influenced variability in ECF. In the senescing group, the decline in ECF corresponded to atrophic changes in cerebral WM (sulcal and intergyral span) primarily in the superior frontal and anterior cingulate regions. A large fraction of the variability in ECF (62%) can be explained by variability in the structural indices from these two regions. *Hum Brain Mapp 30:2581–2594, 2009.* © 2008 Wiley-Liss, Inc.

Key words: aging; morphology; cerebral health; atrophy; maturation

INTRODUCTION

The upcoming decades will be marked by substantial increases in the proportion of population above 65 years of age [He et al., 2006]. This rapidly growing segment of the population is characterized by rising prevalence of cognitive impairment and disabilities. There is an urgent need for sensitive measures of the aging process to better understand the neurobiology of cognitive decline in this age group. Such measures may ultimately be used (1) for gauging factors that affect aging and neurodegenerative processes, (2) for assessment of genetic factors that predispose one to abnormal aging, and (3) for clinical trials that determine the therapeutic value of anti-dementia drugs and their ability to resist degenerative changes. A better

Contract grant sponsor: National Institute of Biomedical Imaging and Bioengineering; Contract grant number: K01 EB006395; Contract grant sponsor: NIMH, NIDA (Human Brain Mapping Project); Contract grant number: P20 MH/DA52176; Contract grant sponsor: General Clinical Research Core; Contract grant number: M01 RR01346.

*Correspondence to: Peter Kochunov, Ph.D., University of Texas Health Science Center at San Antonio, Research Imaging Center, 7703 Floyd Curl Drive, San Antonio, Texas 78284.
E-mail: kochunov@uthscsa.edu

Received for publication 22 April 2008; Revised 29 September 2008; Accepted 8 October 2008

DOI: 10.1002/hbm.20689

Published online 9 December 2008 in Wiley InterScience (www.interscience.wiley.com).

understanding of cerebral aging requires a broad perspective that can be achieved by combining cognitive (behavioral) and noninvasive brain imaging methods, thereby providing data to guide development of comprehensive, neurobiologically realistic models of aging.

As an initial step in the development of such neurobiological models, we investigated whether neuroimaging-based indices of structural integrity could explain a significant portion of individual variation in executive control function (ECF). ECF was chosen because of its importance to normal cognitive functioning and dementia, as it facilitates planning and adaptation to novel situations, and regulates complex goal-driven actions [Collette et al., 2005, 2006]. Another advantage of using ECF is that associated neuroanatomical networks are generally well mapped. Lesion studies, and more recently functional imaging studies, have localized ECF and its deficits predominantly to frontal and cingulate regions [Collette et al., 2005, 2006; Royall et al., 2001].

Association between neuropsychological status and degree of cerebral atrophy has been studied in clinical populations affected with Alzheimer's disease, ischemic brain disorder, and multiple sclerosis [Csernansky et al., 2005; Du et al., 2005b; Ezekiel et al., 2004; Royall et al., 2001]. However, these disorders are generally characterized by more dramatic changes in neuropsychological status and in measurements of cerebral integrity. Finding an association between changes in neuropsychological measures with changes in regional cerebral integrity has been challenging in normal subjects because of the subtleness of these changes. Another challenge in studies of ECF in normal subjects is that ECF-sensitive measures follow a nonlinear, ''U-shaped'' trajectory with age. During cerebral maturation, the ECF improves with age reaching maturity levels in the 3rd–4th decades of life and then declines in later decades [Royall, 2000].

We used the following neuroimaging-based structural indices to study variability in ECF in healthy maturing and senescing individuals: Gray matter (GM) thickness, the width of intergyral span, the width of intrasulcal CSF spaces, fractional anisotropy (FA) of cerebral WM, and the volume of the T2-hyperintense white mater (HWM). Each anatomical measure are described below.

GM thickness is a neuroimaging marker of cortical integrity related to regional neuronal density in the cortical mantle [Jelsing et al., 2005; Lerch and Evans, 2005; Selemon et al., 1995]. Age-related changes in cortical thickness are well described [Sowell et al., 2003]. In normal subjects, the average thickness of the gray matter mantle follows an inverted-U trajectory with age: GM thickness rises during maturation, reaching maximum during the 2nd and 3rd decades of life and then decreases linearly with age [Kochunov et al., 2007, 2008; Magnotta et al., 1999; Raz N et al., 1997]. The rate of cortical GM thickness reduction in abnormal aging could be different from that in healthy aging, and this difference could be an important diagnostic factor [Thompson et al., 2003, 2004].

Intergyral span is sensitive to changes in the volume of gyral WM that form the bulk of cortical gyri [Kochunov et al., 2005b]. Sulcal span is a measurement of dilatation of cortical sulci and the compensatory filling of the freed space by CSF. Age-related ''widening'' of cortical sulci was shown to be due to reduction in GM thickness and gyral WM volumes [Jernigan et al., 2001; Kochunov et al., 2005b; Magnotta et al., 1999; Symonds et al., 1999]. Visual assessments of regional ''widening'' of cortical sulci, specifically in the hippocampal, enthorhinal, and medial temporal cortices, are correlated with cognitive decline in mild cognitive impairment and dementia [Bastos Leite et al., 2004].

FA in cerebral WM is a sensitive index of regional breakdown of the microstructure of WM tracts. Global and regional decline in FA has been shown to be correlated with the progression and severity of various degenerative WM disorders such as multiple sclerosis, leukoaraiosis, and various dementias [Horsfield and Jones, 2002]. Previously we reported that FA values decrease during normal aging and that whole-brain average FA values were highly correlated with other indices such as GM thickness and sulcal span [Kochunov et al., 2007]. We also observed that FA values of the thinly myelinated associative tracks had the greatest decline with age and the highest correlation with GM thickness and sulcal span [Kochunov et al., 2007].

HWM lesions, observed as regions of high signal intensity on T2-weighted MR studies, are often present in both normal aging individuals and patients affected with neurodegenerative disorders. HWM lesions arise from regions of accumulation of extra-cellular water associated with degradation of the myelin sheath of nonspecific etiology [Pantoni and Garcia, 1995]. The prevalence of HWM lesions has been reported to be as high as 60–100% in normal subjects 60 years old and older [de Leeuw et al., 2001, 2005]. These lesions appear at a greater extent in frontal regions [Fazekas et al., 2005; Raz et al., 2003] and their volume is correlated with global decreases in cerebral blood flow [Kraut et al., 2008; ten Dam et al., 2007], reduction in cerebral WM and GM volumes [Du et al., 2005a; Wen et al., 2006] and reduction in global and regional FA values [Kochunov et al., 2007].

In this study, we predicted that the five neuroimaging-based markers of structural integrity would partly explain intersubject variability in a sensitive executive control measure, the Executive Interview (EXIT) [Royall et al., 1992, 1994; Stokholm et al., 2005]. The EXIT provides a standardized assessment of ECF. It takes ~15 min to administer, has high internal consistency ($r = 0.85$), high inter-rater reliability ($r = 0.90$) [Chan et al., 2006; Royall et al., 2007] and is available in multiple language translations [Chan et al., 2006; Stokholm et al., 2005]. EXIT scores have been shown to correlate well with performance on other ECF-sensitive tests, such as the Wisconsin Card Sorting Task (WCST) ($r = 0.54$), trail making part B ($r = 0.64$), Lezak's tinker toy test ($r = 0.57$), and the test of sustained attention (time, $r = 0.82$; errors, $r = 0.83$). However, EXIT scores

appear most strongly associated with cognitive disability and clinical outcomes [Lewis and Miller, 2007; Royall et al., 2003, 2007]. In normal aging populations, performance on EXIT was associated with both cross-sectional level of care [Royall et al., 2000, 2003], and longitudinal change in instrumental activities of daily living [Royall et al., 2004, 2005a]. Performance on EXIT was also shown to predict other clinically relevant outcomes such as medication compliance and medical decision making capacity [Allen et al., 2003; Dymek et al., 2001]. Important advantages of the EXIT include its brevity and its validity in older populations. Moreover, unlike the WCST, the EXIT has no appreciable learning effect, and is sensitive to change in repeated measures designs [Royall et al., 2005b]. This makes EXIT feasible for assessing and monitoring ECF in combination with neuroimaging-based measurements of cerebral integrity during studies of normal and neurodegenerative aging, treatment effects, and clinical interventions.

METHODS

Subjects

Seventy one (44 females, 27 males), healthy, right handed, 19–90 years of age (average age = 47.4 ± 22.1 years) were recruited as the part of the International Consortium on Brain Mapping (ICBM) project [Mazziotta et al., 1995, 2001]. Subjects were treated as two groups with approximately equal numbers per group, maturing, younger (age 19–29, N = 33, 21/12 females/males), and senescing, older (age 30–90, N = 38, 23/12 females/males). Subject's medical history was reviewed to rule out endocrinal, neurological, and psychiatric illnesses. The study was performed with institutional review board approval, and subjects provided written informed consent. All neuropsychological testing and brain imaging was performed at the Research Imaging Center, University of Texas Health Science Center at San Antonio.

MR Imaging

MR imaging was performed at the Research Imaging Center, UTHSC, using a Siemens 3T Trio scanner and a high-resolution 8-channel head coil.

T1-weighted imaging

High-resolution (isotropic 800 μm), T1-weighted images were acquired using a retrospective motion-corrected protocol [Kochunov et al., 2006]. Under this protocol, seven full-resolution volumes are acquired using a 3D Turbo-FLASH sequence with an adiabatic inversion magnetization preparation contrast pulse (scan parameters: TE/TR/TI = 3.04/2100/785 ms, flip angle = 11 degrees). The sequence yields uniform tissue contrast across the imaging volume. Imaging time was 26 min.

Diffusion weighted imaging

Single-shot, spin-echo, echo-planar gradient recalled echo, T2-weighted, sequence was used to acquire diffusion weighted data with the spatial resolution of 1.7 × 1.7 × 3.0 mm^3. The sequence parameters were TE/TR = 87/8000ms, with 86 diffusion weighted directions and two diffusion weighing values of 0 and 700 s/mm^2. The total sequence acquisition time was 12 min.

T2-weighted imaging

The T2-weighted data were acquired with a high-resolution (isotropic 1 mm), 3D turbo-inversion recovery Fluid Attenuated Inversion Recovery (FLAIR) sequence with the following parameters: TR/TE/TI/Flip angle = 5 s, 353 ms, 1.8 s, 180 degrees. This sequence uses a nonselective inversion recovery pulse to prevent CSF pulsation artifacts [Bakshi et al., 2000]. Imaging time was 15 min.

Structural Image Processing

Structural image processing consisted of preprocessing of T1-weighted images, sulcal surface analysis, and processing of FA and HWM images.

Preprocessing of T1-weighted images

Preprocessing of T1-weighted images consisted of removing nonbrain tissues, global spatial normalization, and radio frequency (RF) inhomogeneity correction. Nonbrain tissues such as skin, muscle, and fat were removed using an automated skull stripping procedure provided by the brain extraction tool [Smith, 2002] (see Fig. 1A). The extracted brain images were cropped at the level of the cerebellum. Next all brain images were globally spatially normalized to the Talairach coordinate system to remove gross differences in brain location, size, and orientation. Automated, nine-parameter (three rotations, three scales, three translations) FSL FLIRT global spatial normalization software [Smith et al., 2004] was used to register all images to a Talairach template [Kochunov et al., 2002]. All images were resliced to isotropic 800 μm spacing using a 3D, 15-voxel-wide sinc interpolation kernel. Images were radio frequency (RF) inhomogeneity corrected using the FAST tool (Fig. 1B) [Zhang et al., 2001]. Default FAST parameters were used. RF corrected images were imported into the BrainVISA database and processed through its sulcal extraction and identification pipelines, as described by Kochunov et al., [2005].

Sulcal surface processing

The BrainVISA image processing pipeline extracts hemispheric spherical meshes from segmented gray and white matter images (Fig. 1C,D). The medial surface of the cortical in-folds is obtained using a homotopic erosion technique [Mangin et al., 1995]. A ''crevasse detector'' is used to reconstruct sulcal structures as the medial surfaces from

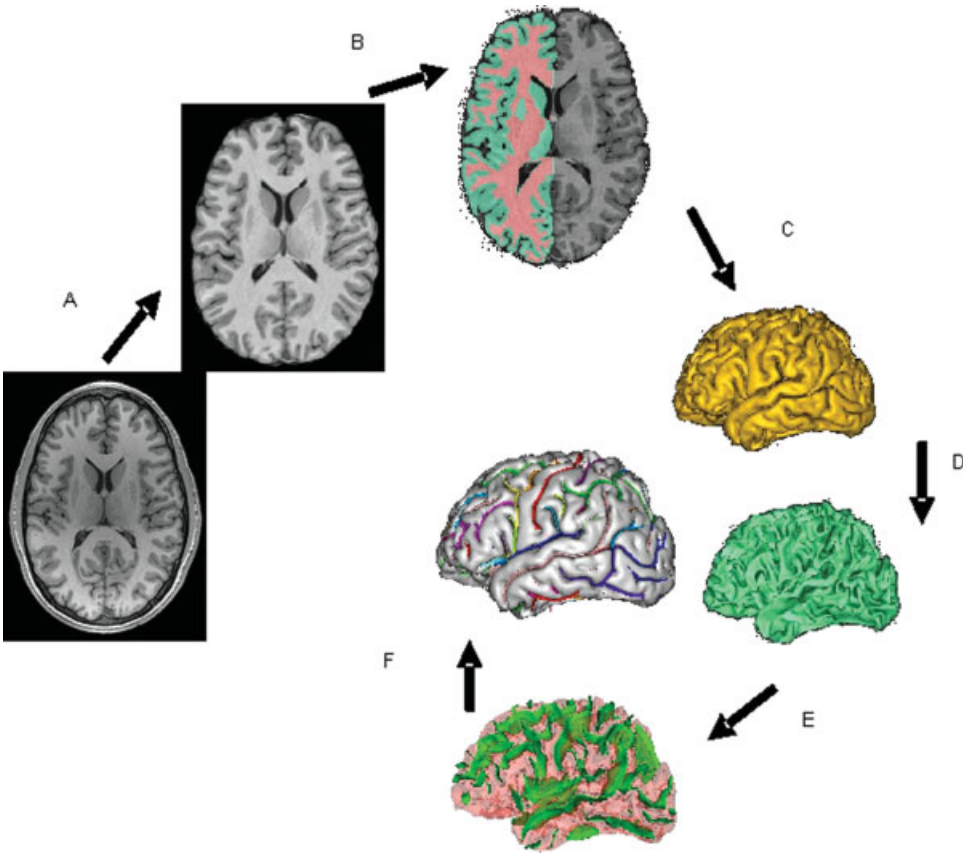

Figure 1.

T1-weighted image processing pipeline for extraction of indices of cortical integrity consists of skull stripping (**A**); spatial normalization, radio-frequency homogeneity correction, and tissue segmentation (**B**); extraction of gray and white matter surfaces (**C**,**D**) extraction of sulcal folds (**E**); and automated labeling of sulci (**F**).

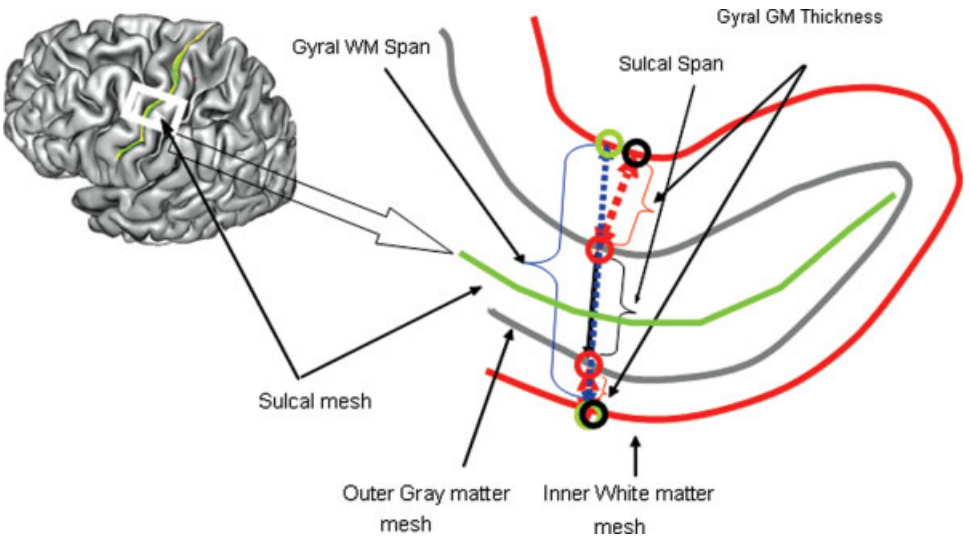

Figure 2.

TABLE I. Gyral gray matter thickness, sulcal and gyral spans were calculated for five cortical regions per hemisphere based on 12 primary and secondary sulcal structures per hemisphere

Region	Sulcal structures and brodmann areas (BA)
Superior frontal/anterior cingulate	Superior frontal sulcus (BA 46/9/8); anterior cingulate sulcus(BA 24/32)
Primary somatosensory	Pre-central sulcus; postcentral sulcus; central sulcus (BA 6/4/3/1/2)
Parietal/post.cingulate	Intraparietal fissure (BA 19/39); posterior cingulate sulcus (BA 23/31)
Temporal	Superior temporal sulcus (BA22/21); collateral sulci(BA20/36)
Occipital	Occipital/calcarine sulci(BA 17/18); parietaloccipital fissure(BA 7/19)

two opposing gyral banks that span from the most internal point of the sulcal fold to the convex hull of the cortex [Mangin et al., 1995, 2004] (Fig. 1E). The BrainVISA sulcal identification pipeline incorporates a congregation of 500 artificial neural network-based pattern classifiers. Each classifier is tuned to identify a particular feature of the sulcal patterns. The neural networks work collaboratively to identify 56 sulcal structures for each hemisphere. The networks were trained on a database of 26 expertly classified images. Classification accuracy ranged from 95% for primary and secondary fissures to around 70% for the highly variable tertiary sulcal structures [Rivière et al., 2002]. Two skilled neuroanatomist reviewed the results of the automated sulcal identification. In an infrequent event (~5–15%) where a sulcus was assigned an incorrect label, the sulcus was manually relabeled while overlaid on the cortical surface (Fig. 1F). Special attention was paid to anastomotic sulci, small, accessory sulci, usually less than 5 mm in length [Ono et al., 1990]. Anastomotic sulci were excluded from analysis because a span measurement performed at intersections between anastomotic and targeted sulci, especially along the direction of the anastomotic sulcus, would lead to exaggerated values.

Five cortical regions were composed from twelve cortical sulci by grouping functionally similar sulci (Table I). Sulci selected for this analysis were previously used to study age-related changes during senescence [Kochunov et al., 2005b]. All sulci have very high inter-subject incidence rates (~99%) [Ono M et al., 1990] and were present in all subjects.

FA processing

We used the tract-based spatial statistics (TBSS) software [Smith et al., 2006] for multi-subject analysis of FA [Kochunov et al., 2007]. TBSS combines strengths of voxel-wise [e.g., VBM—voxel based morphometry [Ashburner and Friston, 2000] and WM tractography methods. During TBSS processing, FA images were created by fitting the diffusion tensor to the raw diffusion data [Smith, 2002]. Then, all FA images were nonlinearly aligned to a group-wise, minimal-deformation target (MDT) brain. The group's MDT brain was identified by warping all individual brain images in the group to each other [Kochunov et al., 2001]. Individual FA images were averaged to produce a group-average anisotropy image. This image is used to create a group-wise skeleton of white matter tracts. Finally, FA images were projected onto the group-wise skeleton of white matter structures. This step accounted for residual misalignment among individual white matter tracts. In the last step, we used a threshold FA value of 0.2 to reconstruct fully connected skeleton for even the eldest subjects where FA values were generally lower.

HWM processing

Hyperintense white matter (HWM) volume was measured from T2-weighted FLAIR images as described by Kochunov et al., [2007]. FLAIR images were preprocessed by removal of nonbrain tissue, registration to the T1-weighted images/Talairach frame, and RF inhomogeneity correction.

Structural Indices of Cerebral Integrity

Descriptions of methods for measurements of global and regional indices of cerebral integrity were published elsewhere [Kochunov et al., 2005b, 2007, 2008). Cortical cerebral integrity measurements, sulcal, intergyral span, and GM thickness were performed for five regions (Table I); FA values were measured for the entire brain and three regions of corpus callosum; HWM volume was calculated for the entire brain.

Sulcal span

Sulcal span was defined as the average span of the sulcal space along the normal projections to the medial sulcal mesh (see Fig. 2). High resolution medial sulcal meshes for each sulcus were created using the BrainVISA sulcal extraction pipeline. Geometrically, a medial sulcal mesh

Figure 2.

Three indices of cortical integrity were measured for primary cortical sulci (Table I). The sulcal surface is defined as a surface that spans the median space between two gyral banks. Three measurements are computer per sulcal structure: Average sulcal and intergyral spans. A sulcal span (solid line) was defined as a 3D distance between opposing points on the GM mesh along the normal projections to the medial sulcal mesh. A intergyral span (dotted line) was defined as the 3D distance between opposing points on the WM mesh along the normal projection to the medial sulcal mesh. These measurements are performed for all nodes of the individual sulcal mesh, resulting in averaging of ~2–5000 measurements for each sulcal structure.

traverses the sulcal space in the middle of the sulcal ''span'' dimension, parallel to the gyral gray matter borders, and spans the entire sulcal ''depth'' dimension (see Fig. 2). The medial sulcal mesh for each sulcus was used to seed a 3D region growing algorithm to mask cerebrospinal fluid volume associated with the sulcal structure (see Fig. 2). To prevent cerebrospinal fluid from ''spilling over'' into intersecting sulci, points that were further than 10 mm away from the sulcal skeleton were rejected. The convex hull of the cortical gray matter ribbon was then used to isolate sulcal space from subarachnoid cerebrospinal fluid. Sulcal span was calculated as the Euclidean distance between two points on the gyral gray matter mesh on either side of the sulcal surface (see Fig. 2). The point of intersection between the normal projection and the gray matter mesh corresponded to voxels with partial cerebrospinal fluid/gray matter values of 50%.

Intergyral span

Intergyral span was calculated by extending the sulcal span tracings until they intersected with the surface corresponding to the gyral gray matter-white matter interface. Gyral span was defined as the Euclidean distance between two points residing on the gyral white matter mesh on either side of the sulcal surface (see Fig. 2).

Gray matter thickness

Gray matter thickness was calculated by starting a new tracing at the point of intersection between a normal projection to the sulcal mesh and the exterior gray matter mesh. To measure GM thickness, a normal projection to the exterior gray matter mesh was traced until it intersected with the interior gray matter mesh that describes the gray matter-white matter interface (see Fig. 2). The point of intersection between the normal projection and the interior gray matter mesh corresponds to voxels with partial white matter/gray matter values of ~50%.

Fractional anisotropy

FA values were measured as the whole brain average and for three regions of the corpus callosum (CC) subdivided along its anterior–posterior length [Kochunov et al., 2005a]. The whole brain FA average value was calculated for all voxels of the skeleton. Regional CC FA values were calculated from a 10 mm wide band of median CC. This band was subdivided along the A-P direction into three equal subparts: Genu, midbody. and splenium. Studies in cadavers indicated that the genu (anterior third) contains the thinly myelinated, tightly packed association fibers connecting the bilateral prefrontal cortices; the midbody (middle third) primarily contains thickly myelinated fibers for motor, somatosensory, and auditory cortices; and the splenium (posterior third) contains a mixture of heavily myelinated and thinly myelinated fibers connecting temporal, parietal, and occipital lobes[Aboitiz, 1992; Aboitiz et al., 1992; Highley et al., 1999].

HWM volume

Regions of HWM were manually delineated (painted) on the FLAIR images by two experienced neuroanatomists with high (r = 0.85) inter-rater reliability. HWM volume was calculated by adding volumes of individual regions.

Statistic analysis

Normality of EXIT scores and cerebral integrity indices was tested by Shapiro-Wilk's and Kolmogorov-Smirnov tests. Logarithmic transformation was used to achieve normality for the EXIT scores and HWM volume. Linear and age-corrected partial correlation analysis was used to examine relations among indices of structural integrity and normalized EXIT Scores (NES). Only the indices that showed significant age-corrected correlation with NES were selected for the further analysis. This selection criterion allowed us to study age-independent association between structural indices and cognition. It also allowed for the reduction of the number of dependent variables prior to factor analysis to achieve a ratio of dependent variables to the number of subjects ratio of at least 1:10 [Osborne and Costello, 2004]. Factor analysis was performed to further reduce the number of dependent variables and to remove the colinearity among the indices of cerebral integrity to satisfy the requirements of regression analysis. Factor analysis used the principal components analysis (PCA) to obtain linear composites of correlated variables. It yielded eigenvector values describing correlations between a variable and a component. A varimax rotation was then used to remove colinearity e.g., to orthogonize the individual eigenvectors. Results of factor analysis yielded factor loadings (correlations between a variable and a factor) and factor scores (a subject's standardized score on each factor). Finally, a two-stage regression was performed to probe the multivariate effects of age and structural indices of cerebral integrity on the inter-subject variability in NES. Subject age was entered at first, followed by the factor scores extracted from structural measurements. The regression analysis yielded the degree of variance described at each entry step and whether the change was significant. It also produced standardized coefficients (β) that estimate linear associations between criterion variables (NES) and predictor variables (factor scores extracted from the structural indices).

RESULTS

Normalized EXIT Scores

In the maturing group, raw EXIT scores ranged from 3 to 16 (average = 7.5 ± 2.7); in the senescing group raw EXIT scores ranged 5–25 (average = 12.8 ± 5.0). EXIT scores were adjusted using logarithmic transformation to

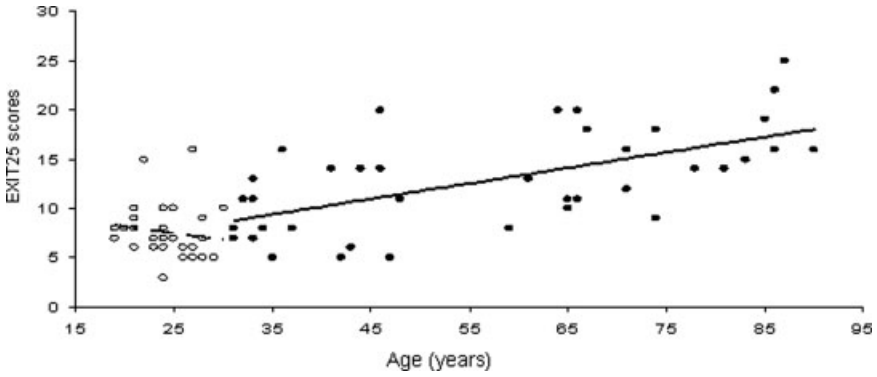

Figure 3.
Age-related trends for Executive Interview scores for maturing (○, dotted line), age 19–29 and senescing (●, solid line), age 30–90 years subjects.

achieve normality, producing normalized EXIT scores (NES) that satisfied this criteria (maturing group: Shapiro-Wilk's $w = 0.95$, $P = 0.13$; Kolmogorov-Smirnov $F = 0.13$, $P = 0.19$; senescing group: Shapiro-Wilk's $w = 0.94$, $P = 0.13$; Kolmogorov-Smirnov $F = 0.13$, $P = 0.15$).

Average NES values were significantly different between groups (1.96 ± 0.06 maturing group; 2.5 ± 0.07 senescing group; $t = 5.5$; $P < 1e\text{-}5$). In addition, age-related slopes for NES were opposite in sign between the maturing and senescing groups (see Fig. 3), and the between-group difference in correlation coefficients with age was highly significant (Fisher's $z = 3.7$; $P < 0.001$). Younger subjects showed a nonsignificant negative correlation between NES and age, hinting that performance on the test improved with age. NES were positively and significantly correlated with age in the senescing group; tracking an expected decline of ECF with age (Table II; Fig. 3).

Whole-Brain Indices of Cerebral Integrity

Whole-brain average measurements of cerebral integrity (GM thickness, intergyral and sulcal spans, FA, and HWM volume) were significantly correlated with age in the senescing group (Table II; Fig. 4A–C; Fig. 5B). In the maturing group, only the FA measurements in the genu of CC showed a statistically significant correlation with age (Figures 4A–C, 5A). Partial correlation analysis was used to probe age-independent trends between NES and whole-brain average measurements. The only significant age-independent correlation was between NES and the whole brain average sulcal span in the senescing group (Table III).

Regional Indices of Cerebral Integrity

The results of uncorrected and age-corrected correlation analyses between NES and three indices of cerebral integrity (GM thickness, intergyral, and sulcal spans) for five cortical regions for two hemispheres are presented in Tables IV and V. The level of statistical significance was set at $P = 0.001$ to reduce the probability of Type 1 errors associated with 30 (three measurements * five regions * two hemispheres) comparisons.

In the maturing group, none of the 30 cortical integrity measurement showed a significant ($P < 0.001$) correlation with NES. However, there were marginally significant correlations ($P \sim 0.01$) observed between NES and right and left sulcal span in the occipital region (Table IV).

In the senescing group, 13 of 30 cortical integrity measurements were significantly ($P < 0.001$) correlated with NES (Table V). Age-corrected correlation analysis revealed three regional measurements that correlated with NES at $P < 0.001$ (left and right sulcal span and right hemispheric

TABLE II. Linear correlation coefficients (r) between subject's age and normalized executive interview scores (NES); and whole-brain indices of cerebral integrity

Correlation with age	NES	GM thickness	WM span	Sulcal span	FA	FA genu	FA body	FA splenium	HWM volume
Maturing group	−0.21	−0.11	−0.25	−0.19	0.15	0.40*	0.19	0.31	N/A
Senescing group	0.60*	−0.61*	0.49*	0.68*	−0.53*	−0.63*	−0.38*	−0.51*	.37*

HWM volume could not be measured for younger subjects.
*Indicated statistically significant ($P < 0.05$) correlation coefficients.

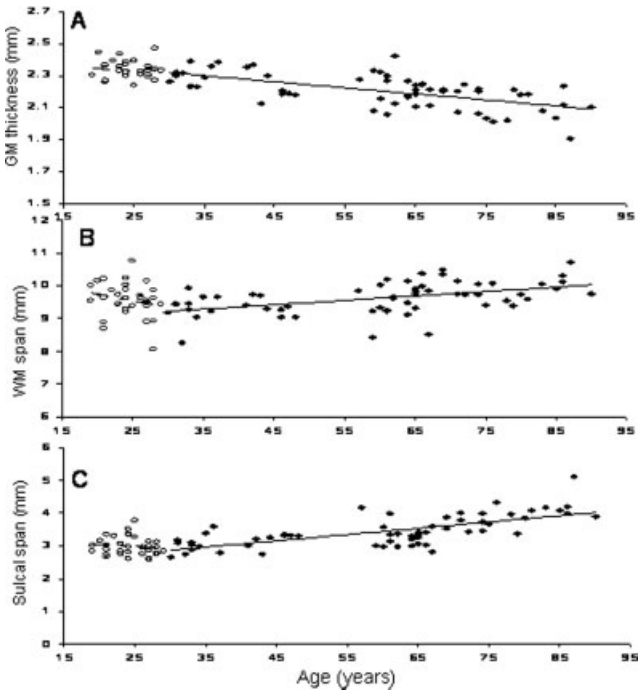

Figure 4.
Age-related trends for average cortical indices of cerebral integrity: GM thickness (**A**), WM span (**B**), and Sulcal Span (**C**) for the maturing (○), age 19–29 and senescing (●), age 30–90 years subjects.

intergyral span in the superior frontal/anterior cingulate region).

Factor Analysis

Factor analysis was performed in senescing group for regional cortical indices that showed a significant ($P < 0.001$) age-corrected partial correlation with NES (Table VI). Factor 1 loaded on left and right sulcal span measurements for the superior frontal/anterior cingulate sulcus. It was significantly and positively correlated with NES, pr = 0.61; $P < 0.001$. Factor 2 loaded on intergyral span measures for the right superior frontal/anterior cingulate sulci. It was also significantly and positively correlated with the NES, pr = 0.57, $P < 0.001$.

Regression Analysis

A two-stage regression analysis was performed in the senescing group. NES was used as the dependent variable and was regressed versus age and the two factor scores. In the first stage, age was entered as the only independent variable. In the second stage, factor scores were entered as independent variables using a step-wise procedure. Age and factor scores produced statistically significant changes in r ($\Delta r \geq 0.33$; $P \leq 0.01$). However, the regression coefficient (β) for age was not significant, indicating that factor scores extracted from structural measurements fully captured age-related variability in NES (Table VII).

DISCUSSION

This study sought to explore the relationship between cognition and indices of cerebral integrity in normally aging subjects. Our results support a multimodal MRI approach to help predict cognitive changes in normal aging. As noted in the introduction, Royall et al., [2000] have previously shown a inverse ''U'' relationship between the EXIT and age, that peaks in the 3rd to 4th decade of life [Royall, 2000]. In the current study, trends in the EXIT scores showed that ECF improved with age in the younger, maturing group and declined in the older, senescing group, thereby replicating the previous work. Parallel to ECF trends, indices of cerebral integrity hinted at developmental trends in the maturing group and showed an age-related decline in the senescing group.

In the maturing group, age-related trends in NES and indices of cerebral integrity hinted at ongoing cerebral development, possibly because of late myelination of associative white matter tracts. This was exemplified by the increasing FA values in the genu of the CC, which is composed of thinly myelinated, densely packed, associative commissural fibers that link prefrontal and frontal areas [Aboitiz, 1992; Aboitiz et al., 1992]. An age-related increase in the genu's FA values in maturing subjects was reported

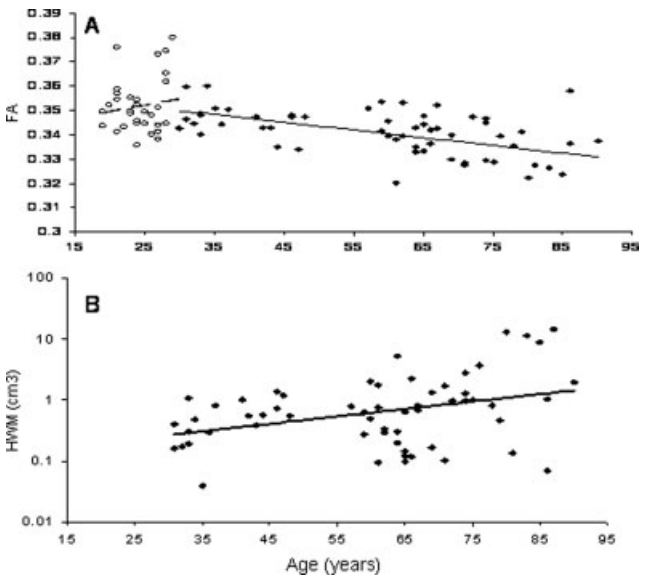

Figure 5.
Age-related trends for average subcortical indices of cerebral integrity: Average fractional anisotropy of water diffusion (**A**) and volume of hyperintense white matte for the maturing (○), age 19–29 and senescing (●), age 30–90 years groups of subjects.

TABLE III. Partial, age-corrected correlation coefficients (pr) between normalized executive interview scores (NES) and indices of cerebral integrity

Correlation with NES	GM thickness	WM span	Sulcal span	FA	FA genu	FA body	FA splenium	HWM volume
Maturing group	0.06	0.15	0.31	−0.17	−0.08	−0.14	−0.17	N/A
Senescing group	−0.04	0.22	0.36*	−0.23	−0.21	0.03	−0.20	0.27

HWM volume could not be measured for younger subjects.
*Indicated statistically significant ($P < 0.05$) correlation coefficients.

to be an indication that the associative WM tracts continue to develop into the third decade of life [Abe et al., 2002; Huppi et al., 1998; Sullivan et al., 2001]. In contrast, FA values in the body of CC were not significantly correlated with age (Table II). This was expected as the fiber tracts located in the body of CC are composed of heavily myelinated motor and sensory fibers, known to myelinate at an early age [Kochunov et al., 2005a]. We also believe that the observed, albeit not statistically significant, age-related decrease of the intergyral span is further evidence of late myelination. We tested this observation by analyzing the correlation between the intergyral span and FA measurements in the genu of CC, which was highly significant ($r = -0.55$; $P <$ 1e-3). In contrast, the correlation between intergyral span and FA values in the body of CC was not significant ($r = -0.12$; $P = 0.5$). These results suggest that NES and indices of cerebral integrity were sensitive to cerebral maturation in the younger group.

In the senescing group, age-related trends in NES and indices of cerebral integrity indicated a decline in cognition with a corresponding decline in cerebral integrity. NES and all cerebral indices showed statistically significant ($P < 0.05$) correlation with age (Table II). The highest correlation with age was observed for sulcal span ($r = 0.68$), followed by FA in the genu of the CC ($r = -0.63$) and GM thickness ($r = -0.61$). The smallest correlations were seen for the HWM volume and FA measurements for the body of CC (Table II). Interestingly, FA in the genu of CC was the only cerebral index that showed statistically significant association with age in both maturing and senescing groups, suggesting that FA of late-myelinated associative fibers was sensitive to both maturation and senescence.

In the maturing group, regional measures of cerebral integrity were poor at predicting changes in NES (Table IV). We found marginally significant correlation with NES for the sulcal span of occipital areas (age-corrected, pr = 0.38; $P \sim 0.01$) (Table IV; Fig. 6). However, these structures (e.g. left and right occipital structures) were previously reported to have age-related increases in cortical complexity in children ages 6–16 [Blanton et al., 2001]. Blanton et al. hypothesized that changes in axonal tensions due to continuous myelination of associative fibers were the likely cause [Blanton et al., 2001]. We tested their hypothesis by evaluating age-controlled correlation between occipital sulcal span and FA values in the CC. The strongest correlation was observed with the FA of the splenium of the CC (age corrected, pr = −0.44, $P < 0.01$). The splenium of CC contains late myelinating, associative visual-spatial orientation fibers linking occipital and parietal lobes [Aboitiz et al., 1992]. Occipital sulcal span measures also significantly correlated with FA values in the other late-myelinating area of CC, the genu ($r = -0.37$, $P < 0.05$), but were not correlated with FA in the mostly early-myelinated of CC midbody ($r = -0.29$; $P \sim 0.10$). This confirms that maturational changes in occipital areas, first reported by Blanton et al., [2001], are likely due to late myelination of associative WM. Thus, marginally significant correlation between occipital sulcal span and NES is indirect evidence that late-term maturation of cerebral WM influenced variability in ECF in maturing group.

TABLE IV. Uncorrected and age-corrected partial correlation between regional, right (R)/left (L) cerebral integrity indices and normalized executive interview scores for the younger, maturing (age range 19–29, *N* = 34) subjects

Raw and age-corrected partial correlation with NES	R. GM thickness		L. GM thickness		R. WM span		L. WM span		R. sulcal span		L. sulcal span	
	Direct	Partial	Direct	Partial	Direct	Partial	Direct	Partial	Direct	Partial	Direct	Partial
S. Frontal/anterior cingulated	−0.05	−0.05	0.04	0.00	0.04	0.00	0.06	−0.10	0.21	0.18	0.19	0.13
Primary somatosensory	−0.02	−0.05	−0.03	−0.03	−0.02	−0.02	0.18	−0.04	0.18	0.16	0.25	0.22
Parietal/post cingulate	0.03	−0.05	0.06	−0.03	0.17	0.08	0.20	0.17	0.26	0.23	0.19	0.18
Temporal	−0.23	0.11	0.05	−0.03	0.24	0.12	0.14	0.17	0.31	0.30	0.05	0.01
Occipital	−0.35	−0.34	−0.14	−0.15	−0.02	0.06	0.17	0.11	0.42*	0.38*	0.41*	0.38*
Average	−0.13	−0.12	0.02	−0.05	0.08	0.05	0.15	0.06	0.28	0.25	0.22	0.18

*Indicated statistically significant ($P < 0.05$) correlation coefficients.

TABLE V. Uncorrected and age-corrected partial correlation between regional, right (R)/left (L) cerebral integrity indices and normalized executive interview scores (NES) for older (O), senescing (age-range 30–90; *N* = 38) subjects

Raw and age-corrected partial correlation with NES	R. GM thickness		L. GM thickness		R. WM span		L. WM span		R. sulcal span		L. sulcal span	
	Direct	Partial	Direct	Partial	Direct	Partial	Direct	Partial	Direct	Partial	Direct	Partial
S. Frontal/anterior cingulate	−0.34*	−0.08	−0.33*	−0.05	**0.68***	**0.58***	**0.56***	0.33*	**0.67***	**0.61***	**0.62***	**0.54***
Primary somatosensory	−0.**41***	−0.11	−0.35*	−0.09	0.22	0.03	0.31	0.02	**0.57***	0.26	0.**55***	0.26
Parietal/post Cingulate	−0.37*	−0.09	−0.32*	−0.14	0.17	0.02	0.20	−0.08	**0.40***	−0.02	**0.40***	0.11
Temporal	−0.**39***	−0.25	−0.36*	−0.15	0.09	−0.05	0.16	−0.16	**0.55***	0.34	**0.40***	0.13
Occipital	−0.35*	0.03	−0.**48***	−0.11	0.03	**0**.03	0.04	−0.08	0.27	0.11	0.35*	0.11
Average	−0.37	−0.1	−0.36	−0.11	0.23	0.11	0.25	−0.08	0.49	0.26	0.46	0.23

Bolded numbers indicate statistically significant correlations at $P < 0.001$ level.
*Indicated statistically significant ($P < 0.05$) correlation coefficients.

In the senescing group, regional measures of cerebral integrity correctly localized the ECF network and identified specific neuroanatomical correlates predictive of decline in NES (Table IV). Regional measurements of sulcal and intergyral span from frontal and anterior-cingulate areas accounted for 62% of the intersubject variability in NES. Localization of the ECF network to the frontal-cingulate areas is consistent with previous reports from our center [Royall et al., 2001] and others [Collette et al., 2005, 2006; Duncan and Owen, 2000; Vandenberghe et al., 2000]. An important finding was that only sulcal and intergyral spans in the anterior cingulate and superior frontal areas were associated with age-independent decline in NES. Factor analysis distilled these measurements into two orthogonal categories each explaining equal amounts of variance in NES (Table VI). Factor 1 was significantly correlated with two common measures of WM atrophy: The volume of HWM (age-corrected, pr = 0.46; $P < 0.01$) (see Fig. 7] and whole-brain average FA value (age-corrected, pr = −0.45; $P < 0.01$). These associations were expected, as increases in HWM volume are frequently reported to be associated with cognitive decline in normal aging individuals [Gunning-Dixon and Raz, 2000, 2003; Raz et al., 1998]. Factor 2, was significantly correlated with FA values of the genu of the CC (age corrected, pr = 0.34; $P < 0.05$) (see Fig. 8). This is a novel finding suggesting that interhemispheric connections through the genu are associated with a decline in NES.

Limitations

A possible limitation of this study was the use of EXIT as the measure of ECF. ECF is a multidimensional construct comprising a variety of cognitive processes. This would raise the question as to whether the EXIT findings are nonspecific projections from multiple dimensions. However, previous research done by this group and others has shown that the EXIT loads on a specific ECF dimension that is uniquely associated with disability and is not colabeled by either the WCST or trail-making [Park et al., 2006] tests (TMT) [Lewis and Miller, 2007; Royall et al., 2003]. It has also been shown that EXIT scores are closely related to the Tower of London (TOL) and similar cognitive planning tasks strongly associated with measures of functional status [Lewis and Miller, 2007; Royall et al., 1992]. The association between planning and functional status helps to explain the EXIT's singularly strong associations with functional outcomes [Lewis and Miller, 2007]; particularly relative to the WCST or TMT (i.e., putative ECF measures that do not co-label the same ECF factor as the EXIT) and are less strongly associated with functional status [Bell-McGinty et al., 2002]. Another limitation of this investigation was the relatively narrow age range of the maturing, younger group. This restriction could have contributed to the lack of significant findings for this group through a variance compression artifact. In particular, younger subjects had smaller variability in age and NES versus the older group (SD = 2.7 vs 5.0).

TABLE VI. Factor analysis in senescing group

	Factor 1 (60%)	Factor 2 (37%)
R. Sup. Frontal/A. Cingulate sulcal span	0.93	0.36
L. Sup. Frontal/A. Cingulate sulcal span	0.93	0.35
R. Sup. Frontal/A. Cingulate gyral wm span	0.36	0.94

TABLE VII. Two-stage regression result in the senescing group

Model	*r*	Adjusted *r*	Δ*r*	Significance of Δ*r*	Standardized β	Significance of β
Age	0.60	0.58	0.60	<0.01	0.00	0.12
Factor 1	0.68	0.66	0.33	=0.01	0.19	0.001
Factor 2	0.79	0.77	0.35	<0.01	0.18	0.002

Normalized executive interview scores (NES) were used as a dependent variable.Subject's age was entered at the first stage, followed by step-wise insertion of factors 1 and 2 at the second stage.

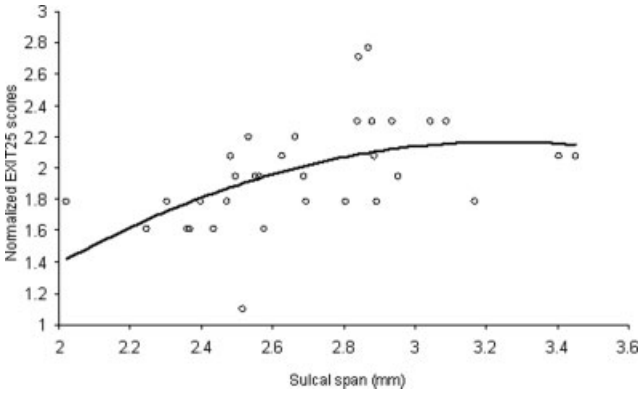

Figure 6.
Age-corrected normalized Executive Interview scores (NES) plotted versus bilateral measurements of sulcal span in occipital region for maturing subjects (age 19–29).

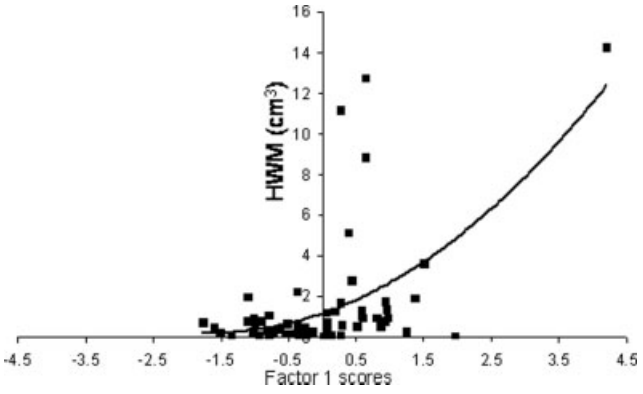

Figure 7.
Factor 1 scores in senescing subjects (ages 30–90) are plotted vs. hyperintense white matter (HWM) volume.

Finally, it is important to consider the statistical approach taken here. We conducted the analyses with categorization of the subjects into two groups. Ideally, this analysis should have been performed by entering subject's age as a continuous variable. Then, a nonlinear regression/correlation analysis could have been used to model the effects of the age as a quadratic or higher-order function. However, the relatively low number of subjects and sparseness of the data in the age range of 35–55 years prevented us from performing a nonlinear analysis. In addition, while subjects from maturing and senescing age groups clearly showed diverging age-related trends for neuropsychological and neuroanatomical measurements (e.g. Figures 4 and 5), these trends have clear linear, rather than higher-order components.

CONCLUSION

We analyzed an association between neuropsychological assessment of ECF and regional indices of cerebral integrity in healthy maturing and sensing populations. In the

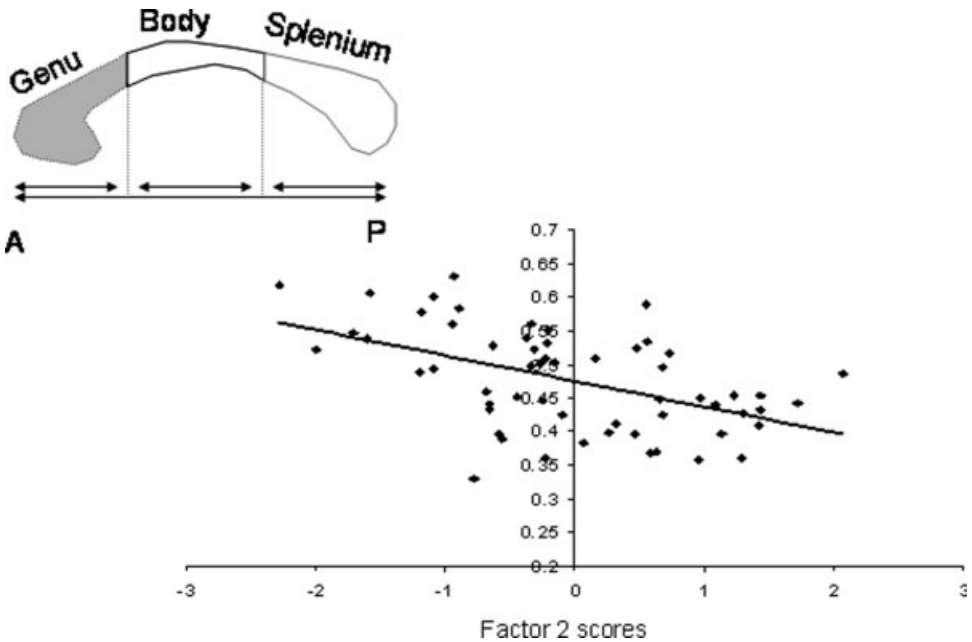

Figure 8.
Average fractional anisotropy values for the genu, shown as the shaded area of the corpus callosum, are plotted versus factor scores for Factor 2 in senescing subjects (age 30–90).

maturing population of 19–29 years old, improvements in ECF corresponded to cerebral maturation trends in the indices cerebral integrity. In the senescing population of 30–90 years old, decline in ECF corresponded to trends in neuroanatomical decline of the indices of cerebral integrity. In both populations, whole-brain trends average cerebral indices did not strongly correlate with trends in ECF. However, regional trends in cerebral markers correlated strongly with trends in ECF. In maturing subjects, the regional pattern of correlation with ECF hinted at late myelination of associative tracks of cerebral WM. In older subjects, regional association patterns included fronto-cingulate structures that were previously reported to be involved in the modulation of ECF. In summary, regional indices of cerebral integrity, corresponding to atrophy of cerebral WM, were highly predictive of deficits in ECF.

REFERENCES

Abe O, Aoki S, Hayashi N, Yamada H, Kunimatsu A, Mori H, Yoshikawa T, Okubo T, Ohtomo K (2002): Normal aging in the central nervous system: quantitative MR diffusion-tensor analysis. Neurobiol Aging 23:433–441.

Aboitiz F (1992): Brain connections: interhemispheric fiber systems and anatomical brain asymmetries in humans. Biol Res 25:51–61.

Aboitiz F, Scheibel AB, Fisher RS, Zaidel E (1992): Fiber composition of the human corpus callosum. Brain Res 598:143–153.

Allen SC, Jain M, Ragab S, Malik N (2003): Acquisition and short-term retention of inhaler techniques require intact executive function in elderly subjects. Age Ageing 32:299–302.

Ashburner J, Friston KJ (2000): Voxel-based morphometry—The methods. Neuroimage 11(6 Part 1):805–821.

Bakshi R, Caruthers SD, Janardhan V, Wasay M (2000): Intraventricular CSF pulsation artifact on fast fluid-attenuated inversion-recovery MR images: analysis of 100 consecutive normal studies. AJNR Am J Neuroradiol 21:503–508.

.Bastos Leite AJ, Scheltens P, Barkhof F (2004): Pathological aging of the brain: An overview. Top Magn Reson Imaging 15:369–389.

Bell-McGinty S, Podell K, Franzen M, Baird AD, Williams MJ (2002): Standard measures of executive function in predicting instrumental activities of daily living in older adults. Int J Geriatr Psychiatry 17:828–834.

Blanton RE, Levitt JG, Thompson PM, Narr KL, Capetillo-Cunliffe L, Nobel A, Singerman JD, McCracken JT, Toga AW (2001): Mapping cortical asymmetry and complexity patterns in normal children. Psychiatry Res 107:29–43.

Chan SM, Chiu FK, Lam CW (2006): Correlational study of the Chinese version of the executive interview (C-EXIT25) to other cognitive measures in a psychogeriatric population in Hong Kong Chinese. Int J Geriatr Psychiatry 21:535–541.

Collette F, Van der Linden M, Laureys S, Delfiore G, Degueldre C, Luxen A, Salmon E (2005): Exploring the unity and diversity of the neural substrates of executive functioning. Hum Brain Mapp 25:409–423.

Collette F, Hogge M, Salmon E, Van der Linden M (2006): Exploration of the neural substrates of executive functioning by functional neuroimaging. Neuroscience 139:209–221.

Csernansky JG, Wang L, Miller JP, Galvin JE, Morris JC (2005): Neuroanatomical predictors of response to donepezil therapy in patients with dementia. Arch Neurol 62:1718–1722.

de Leeuw FE, de Groot JC, Achten E, Oudkerk M, Ramos LM, Heijboer R, Hofman A, Jolles J, van Gijn J, Breteler MM (2001): Prevalence of cerebral white matter lesions in elderly people: A population based magnetic resonance imaging study. The Rotterdam scan study. J Neurol Neurosurg Psychiatry 70:9–14.

de Leeuw FE, Barkhof F, Scheltens P (2005): Progression of cerebral white matter lesions in Alzheimer's disease: A new window for therapy? J Neurol Neurosurg Psychiatry 76:1286–1288.

Du AT, Schuff N, Chao LL, Kornak J, Ezekiel F, Jagust WJ, Kramer JH, Reed BR, Miller BL, Norman D and others (2005a): White matter lesions are associated with cortical atrophy more than entorhinal and hippocampal atrophy. Neurobiol Aging 26:553–559.

Du AT, Schuff N, Chao LL, Kornak J, Jagust WJ, Kramer JH, Reed BR, Miller BL, Norman D, Chui HC and others (2005b): Age effects on atrophy rates of entorhinal cortex and hippocampus. Neurobiol Aging 27:733–740.

Duncan J, Owen AM (2000): Common regions of the human frontal lobe recruited by diverse cognitive demands. Trends Neurosci 23:475–483.

Dymek MP, Atchison P, Harrell L, Marson DC (2001): Competency to consent to medical treatment in cognitively impaired patients with Parkinson's disease. Neurology 56:17–24.

Ezekiel F, Chao L, Kornak J, Du AT, Cardenas V, Truran D, Jagust W, Chui H, Miller B, Yaffe K and others (2004): Comparisons between global and focal brain atrophy rates in normal aging and Alzheimer disease: Boundary shift integral versus tracing of the entorhinal cortex and hippocampus. Alzheimer Dis Assoc Disord 18:196–201.

Fazekas F, Ropele S, Enzinger C, Gorani F, Seewann A, Petrovic K, Schmidt R (2005): MTI of white matter hyperintensities. Brain 128(Part 12):2926–2932.

Gunning-Dixon FM, Raz N (2000): The cognitive correlates of white matter abnormalities in normal aging: A quantitative review. Neuropsychology 14:224–232.

Gunning-Dixon FM, Raz N (2003): Neuroanatomical correlates of selected executive functions in middle-aged and older adults: A prospective MRI study. Neuropsychologia 41:1929–1941.

He W, Sengupta M, Velkoff V, DeBarros K (2006): Current population reports. Special studies. 65+ in the United States: 2005. US Census Report http://www.census.gov/prod/2006pubs/p23-209.pdf.

Highley JR, Esiri MM, McDonald B, Roberts HC, Walker MA, Crow TJ (1999): The size and fiber composition of the anterior commissure with respect to gender and schizophrenia. Biol Psychiatry 45:1120–1127.

Horsfield MA, Jones DK (2002): Applications of diffusion-weighted and diffusion tensor MRI to white matter diseases—A review. NMR Biomed 15:570–577.

Huppi PS, Maier SE, Peled S, Zientara GP, Barnes PD, Jolesz FA, Volpe JJ (1998): Microstructural development of human newborn cerebral white matter assessed in vivo by diffusion tensor magnetic resonance imaging. Pediatr Res 44:584–590.

Jelsing J, Rostrup E, Markenroth K, Paulson OB, Gundersen HJ, Hemmingsen R, Pakkenberg B (2005): Assessment of in vivo MR imaging compared to physical sections in vitro—A quantitative study of brain volumes using stereology. Neuroimage 26:57–65.

Jernigan TL, Archibald SL, Fennema-Notestine C, Gamst AC, Stout JC, Bonner J, Hesselink JR (2001): Effects of age on tissues and regions of the cerebrum and cerebellum. Neurobiol Aging 22:581–594.

Kochunov P, Lancaster JL, Thompson P, Woods R, Mazziotta J, Hardies J, Fox P (2001): Regional spatial normalization: Toward an optimal target. J Comput Assist Tomogr 25:805–816.

Kochunov P, Lancaster J, Thompson P, Toga AW, Brewer P, Hardies J, Fox P (2002): An optimized individual target brain in the Talairach coordinate system. Neuroimage 17:922–927.

Kochunov P, Lancaster J, Hardies J, Thompson PM, Woods RP, Cody JD, Hale DE, Laird A, Fox PT (2005a): Mapping structural differences of the corpus callosum in individuals with 18q deletions using targetless regional spatial normalization. Hum Brain Mapp 24:325–331.

Kochunov P, Mangin JF, Coyle T, Lancaster J, Thompson P, Riviere D, Cointepas Y, Regis J, Schlosser A, Royall DR, and others. (2005b): Age-related morphology trends of cortical sulci. Hum Brain Mapp 26(3):210–20.

Kochunov P, Lancaster JL, Glahn DC, Purdy D, Laird AR, Gao F, Fox P (2006): Retrospective motion correction protocol for high-resolution anatomical MRI. Hum Brain Mapp 27:957–962.

Kochunov P, Thompson PM, Lancaster JL, Bartzokis G, Smith S, Coyle T, Royall DR, Laird A, Fox PT (2007): Relationship between white matter fractional anisotropy and other indices of cerebral health in normal aging: Tract-based spatial statistics study of aging. Neuroimage 35:478–487.

Kochunov P, Thompson PM, Coyle TR, Lancaster JL, Kochunov V, Royall D, Mangin JF, Riviere D, Fox PT (2008): Relationship among neuroimaging indices of cerebral health during normal aging. Hum Brain Mapp 29:36–45.

Kraut MA, Beason-Held LL, Elkins WD, Resnick SM (2008): The impact of magnetic resonance imaging-detected white matter hyperintensities on longitudinal changes in regional cerebral blood flow. J Cereb Blood Flow Metab 28:190–197.

Lerch JP, Evans AC (2005): Cortical thickness analysis examined through power analysis and a population simulation. Neuroimage 24:163–173.

Lewis MS, Miller LS (2007): Executive control functioning and functional ability in older adults. Clin Neuropsychol 21:274–285.

Magnotta VA, Andreasen NC, Schultz SK, Harris G, Cizadlo T, Heckel D, Nopoulos P, Flaum M (1999): Quantitative in vivo measurement of gyrification in the human brain: Changes associated with aging. Cereb Cortex 9:151–160.

Mangin JF, Frouin V, Bloch I, Régis J, López-Krahe J. From 3D magnetic resonance images to structural representations of the cortex topography using topology preserving deformations. J Math Imaging Vis 1995;5:297–318.

Mangin JF, Rivière D, Coulon O, Poupon C, Cachia A, Cointepas Y, et al. Coordinate-based versus structural approaches to brain image analysis. Artif Intell Med 2004;30:77–97.

Mazziotta JC, Toga AW, Evans A, Fox P, Lancaster J (1995): A probabilistic atlas of the human brain: Theory and rationale for its development. The International Consortium for Brain Mapping (ICBM). Neuroimage 2:89–101.

Mazziotta JC, Toga AW, Evans A, Fox PT, Lancaster JL, Zilles K, Woods R, Paus T, Simpson G, Pike B, and others (2001): A probabilistic atlas and reference system for the human brain: International Consortium for Brain Mapping (ICBM). Philos Trans R Soc Lond B Biol Sci. 356:1293–1322.

Ono M, Kubik S, Abernathey C (1990): Atlas of the Cerebral Sulci. New York: Thieme Medical Publishers.

Osborne J, Costello A (2004): Sample size and subject to item ratio in principal components analysis. Pract Assess Res Eval 9:http://PAREonline.net/getvn.asp?v=9&n=11.

Pantoni L, Garcia JH (1995): The significance of cerebral white matter abnormalities 100 years after Binswanger's report. A review. Stroke 26:1293–1301.

Park HJ, Lee JD, Chun JW, Seok JH, Yun M, Oh MK, Kim JJ (2006): Cortical surface-based analysis of 18F-FDG PET: Measured metabolic abnormalities in schizophrenia are affected by cortical structural abnormalities. Neuroimage 31:1434–1444.

Raz N, Gunning FM, Head D, Dupuis JH, McQuain J, Briggs SD, Loken WJ, Thornton AE, Acker JD (1997): Selective aging of the human cerebral cortex observed in vivo: Differential vulnerability of the prefrontal gray matter. Cereb Cortex 7: 268–282.

Raz N, Gunning-Dixon FM, Head D, Dupuis JH, Acker JD (1998): Neuroanatomical correlates of cognitive aging: Evidence from structural magnetic resonance imaging. Neuropsychology 12: 95–114.

Raz N, Rodrigue KM, Kennedy KM, Head D, Gunning-Dixon F, Acker JD (2003): Differential aging of the human striatum: Longitudinal evidence. AJNR Am J Neuroradiol 24:1849–1856.

Rivière D, Mangin JF, Papadopoulos-Orfanos D, Martinez JM, Frouin V, Régis J. Automatic recognition of cortical sulci of the Human Brain using a congregation of neural networks. Med Image Anal 2002;6(2):77–92.

Royall DR (2000): Executive cognitive impairment: A novel perspective on dementia. Neuroepidemiology 19:293–299.

Royall DR, Mahurin RK, Gray KF (1992): Bedside assessment of executive cognitive impairment: The Executive Interview. J Am Geriatr Soc 40:1221–1226.

Royall DR, Mahurin RK, Cornell J (1994): Bedside assessment of frontal degeneration: Distinguishing Alzheimer's disease from non-Alzheimer's cortical dementia. Exp Aging Res 20:95–103.

Royall DR, Chiodo LK, Polk MJ (2000): Correlates of disability among elderly retirees with ''subclinical'' cognitive impairment. J Gerontol A Biol Sci Med Sci 55:M541–M546.

Royall DR, Rauch R, Roman GC, Cordes JA, Polk MJ (2001): Frontal MRI findings associated with impairment on the Executive Interview (EXIT25). Exp Aging Res 27:293–308.

Royall DR, Chiodo LK, Polk MJ (2003): Executive dyscontrol in normal aging: Normative data, factor structure, and clinical correlates. Curr Neurol Neurosci Rep 3:487–493.

Royall DR, Palmer R, Chiodo LK, Polk MJ (2004): Declining executive control in normal aging predicts change in functional status: The freedom house study. J Am Geriatr Soc 52:346–352.

Royall DR, Palmer R, Chiodo LK, Polk MJ (2005a): Executive control mediates memory's association with change in instrumental activities of daily living: The freedom house study. J Am Geriatr Soc 53:11–17.

Royall DR, Palmer R, Chiodo LK, Polk MJ (2005b): Normal rates of cognitive change in successful aging: The freedom house study. J Int Neuropsychol Soc 11:899–909.

Royall DR, Lauterbach EC, Kaufer D, Malloy P, Coburn KL, Black KJ (2007): The cognitive correlates of functional status: A review from the Committee on Research of the American Neuropsychiatric Association. J Neuropsychiatry Clin Neurosci 19:249–265.

Selemon LD, Rajkowska G, Goldman-Rakic PS (1995): Abnormally high neuronal density in the schizophrenic cortex. A morphometric analysis of prefrontal area 9 and occipital area 17. Arch Gen Psychiatry 52:805–818; discussion 819–820.

Smith SM (2002): Fast robust automated brain extraction. Hum Brain Mapp 17:143–155.

Smith SM, Jenkinson M, Johansen-Berg H, Rueckert D, Nichols TE, Mackay CE, Watkins KE, Ciccarelli O, Cader MZ, Matthews PM

and others (2006): Tract-based spatial statistics: Voxelwise analysis of multi-subject diffusion data. Neuroimage 31(4):1487–1505.

Sowell ER, Peterson BS, Thompson PM, Welcome SE, Henkenius AL, Toga AW (2003): Mapping cortical change across the human life span. Nat Neurosci 6:309–315.

Stokholm J, Vogel A, Gade A, Waldemar G (2005): The Executive Interview as a screening test for executive dysfunction in patients with mild dementia. J Am Geriatr Soc 53:1577–1581.

Sullivan EV, Adalsteinsson E, Hedehus M, Ju C, Moseley M, Lim KO, Pfefferbaum A (2001): Equivalent disruption of regional white matter microstructure in ageing healthy men and women. Neuroreport 12:99–104.

Symonds LL, Archibald SL, Grant I, Zisook S, Jernigan TL (1999): Does an increase in sulcal or ventricular fluid predict where brain tissue is lost? J Neuroimaging 9:201–209.

ten Dam VH, van den Heuvel DM, de Craen AJ, Bollen EL, Murray HM, Westendorp RG, Blauw GJ, van Buchem MA (2007): Decline in total cerebral blood flow is linked with increase in periventricular but not deep white matter hyperintensities. Radiology 243:198–203.

Thompson PM, Hayashi KM, de Zubicaray G, Janke AL, Rose SE, Semple J, Herman D, Hong MS, Dittmer SS, Doddrell DM, and others (2003): Dynamics of gray matter loss in Alzheimer's disease. J Neurosci 23:994–1005.

Thompson PM, Hayashi KM, Sowell ER, Gogtay N, Giedd JN, Rapoport JL, de Zubicaray GI, Janke AL, Rose SE, Semple J, and others (2004): Mapping cortical change in Alzheimer's disease, brain development, and schizophrenia. Neuroimage 23 (Suppl 1):S2–S18.

Vandenberghe R, Duncan J, Arnell KM, Bishop SJ, Herrod NJ, Owen AM, Minhas PS, Dupont P, Pickard JD, Orban GA (2000): Maintaining and shifting attention within left or right hemifield. Cereb Cortex 10:706–713.

Wen W, Sachdev PS, Chen X, Anstey K (2006): Gray matter reduction is correlated with white matter hyperintensity volume: A voxel-based morphometric study in a large epidemiological sample. Neuroimage 29:1031–1039.

Zhang Y, Brady M, Smith S (2001): Segmentation of brain MR images through a hidden Markov random field model and the expectation maximization algorithm. IEEE Trans Med Imaging 20:45–57.